AN INVESTIGATION OF THE STRUCTURE BENEATH MAGADI AREA IN SOUTHERN KENYA RIFT USING GRAVIMETRIC DATA

J. G. Githiri[1], J. P. Patel[2], J. O. Barongo[3] and P. K. Karanja[4]
[1,4]Department of Physics, Jomo-Kenyatta University of Agriculture, Science and Technology, Kenya
[2]Department of Physics, University of Nairobi, Kenya
[3]Department of Geology, University of Nairobi, Kenya
E-mail: githirifsc@jkuat.ac.ke

Abstract
Magadi area is located in the southern part of the Kenyan rift, an active continental rift that is part of the East African Rift system. Local seismic activity monitored previously around Lake Magadi revealed an earthquake cluster caused by swarm activity in the rift centre at shallow depths, which was probably triggered by magma movements. There was need for a follow-up to locate any body at depth with sufficient density contrast that may represent magmatic intrusions. Gravity measurements were carried out in 58 established stations and data from 52 other stations merged from existing coverage of previous measurements. Necessary corrections were applied to the gravity data and a Bouguer contour map prepared. Euler deconvolution technique was used to image depth to the causative bodies along selected profiles on the Bouguer anomaly map. Two dimensional gravity forward models of the subsurface structure were generated by using Euler depth solutions in the start models. Among others, a unique body of density of 3.20 gcm^{-3} was modelled on the northern region near little Magadi at a depth of approximately 0.4 km. The location of the body coincides with the area where earthquake swarm occurs. Such a body of high density contrasts may be caused by mafic intrusions into the crust. Discontinuities in Euler solution cluster along the profiles indicated buried faults in the volcanic rift infill. The high seismicity may hence be associated to magma intrusions.

Key words: Gravity, Bouguer anomaly, Euler Deconvolution, Kenya

1.0 Introduction

Magadi area is situated in the southern part of the Kenyan Rift as shown in the location map labelled figure 1. According to Crossley (1979), volcanism in this segment of the rift began at 15 Ma and ceased by 0.8 Ma. The structural evolution took place from 7 Ma with the Nguruman fault activity with the area developing into an asymmetric graben between 4 Ma and 3 Ma. In the period from Pleistocene to Recent, faulting dissecting the rift floor increased in Magadi area when compared to other segments of the Kenyan Rift (Baker, 1986).

Integrated interpretation of geophysical data by Simiyu (1996) as a geological cross-sectional model displays Magadi area as an asymmetric rift graben bordered in the western side by high angle faults of Nguruman escarpment. The basin fills which has a depth of 3.5 km against the Nguruman scarp to the west and 2.0 km to the east is divided into two parts by a horst structure located just beneath Lake Magadi. The southern segment which covers Lake Magadi area and extends to northern Tanzania developed on a craton type lithosphere. This was obscured by imbricated thrust slices and gravitationally collapsed nappes of the Tanzanian Craton and the Mozambique belt (Smith, 1994; Simiyu, 1996). Therefore this pre-existing framework might have influenced the structural geometry of this part of the rift by reactivation of NW-SE to NNW-SSE ductile and brittle Aswa-Nandi-Loita (ANL) shear zone which bounds Lake Magadi at its northern limit. Structural analysis in Magadi area by Atmaoui (1999) revealed important structural orientations features in the southern segment of the Kenyan rift corresponding to normal faults.

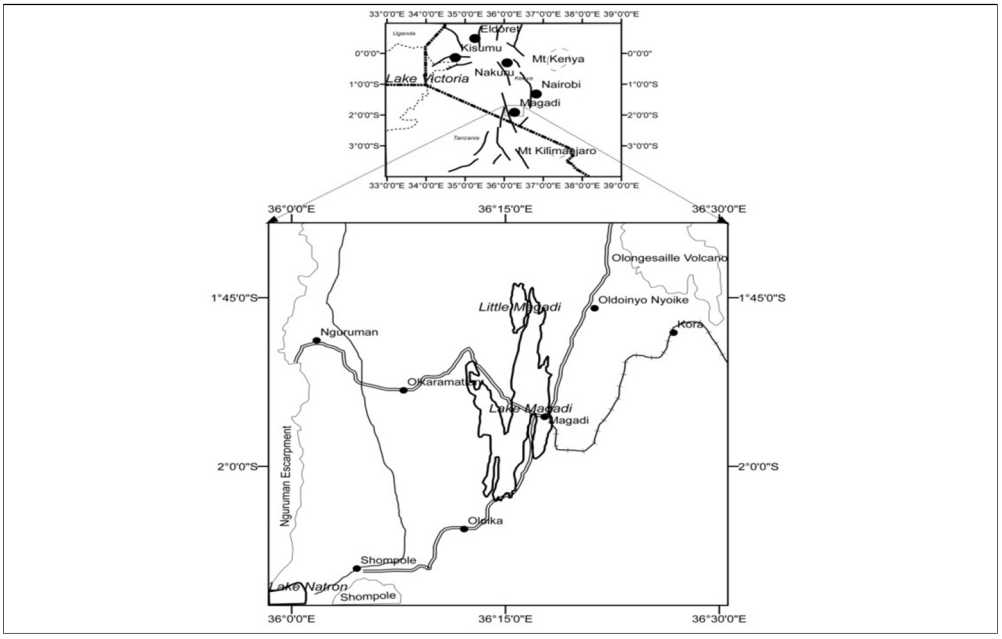

Figure 1: Location map of the study area

The Magadi area is classified into three formations by Baker (1958, 1963) namely Precambrian metamorphic rocks, Plio-Pleistocene volcanics, the Holocene to Recent Lake and fluvial sediments as illustrated in the geological map Figure 2. The basement rocks outcrop in the region west of the Nguruman escarpment. These rocks consist mainly of regular banded schists, gneisses and muscovite-rich quartzites. The basement rocks are overlain by the Kirikiti platform, which is down faulted to the rift floor at the Nguruman escarpment. Baker (1958) found that the olivine basalt layers of the Kirikiti platform are interbedded with conglomerates; gravels and sands deposited between different eruption episodes.The area has three central volcanoes olorgesailie, Oldoinyo Nyokie and Shompole illustrated in figure 1 Olorgesailie being the highest. Its lava composition consists of olivine basalts, alkali trachyte and nephelinite. Further south, Lenderut volcano dated 2.5 Ma has basalt and andesite lavas, while Shompole dated 2.0 Ma consists of carbonatite and nephelinite rocks (Baker, 1963). The most extensive volcanic activity in the area occurred between 1.4 and 0.7 Ma (Crossley, 1979).

2.0 Gravity Data

In this study, gravity measurements were carried out at 58 established stations using a Worden gravimeter and data from 52 other stations were merged from previous surveys sourced from the gravity catalogue of Kenya (Khan and Swain, 1977). Positioning and station elevation were determined using a Global positioning system GPS model Garmin 45. The distribution of the stations is as displayed in figure 3. The projection adopted was the Universal traverse Mercator UTM using Clarke ellipsoid 1880.

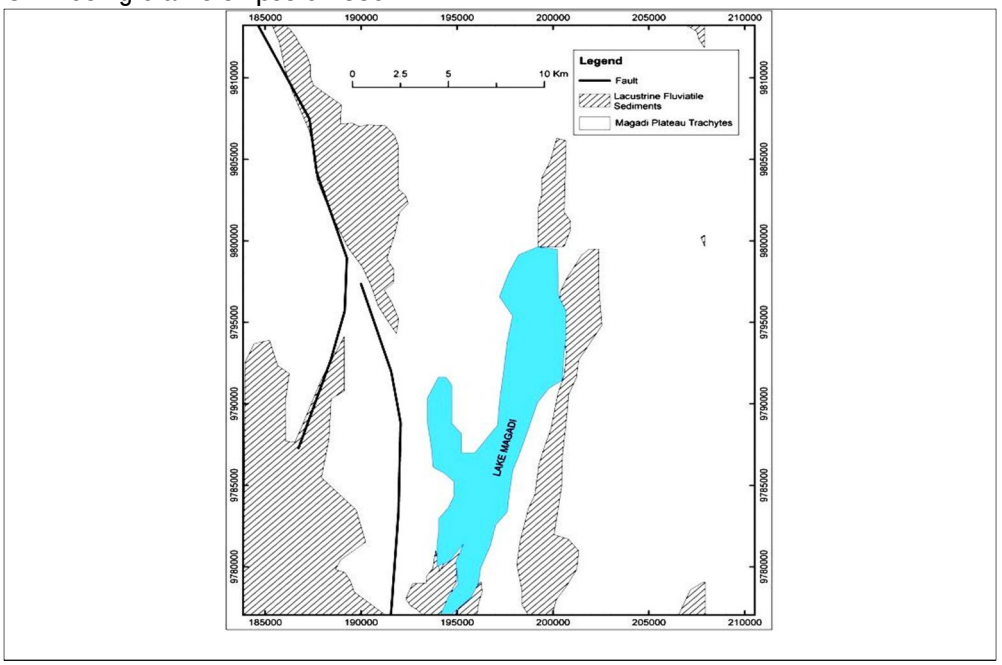

Figure 2: Geological map of Magadi (simplified from Baker, 1958, 1963)

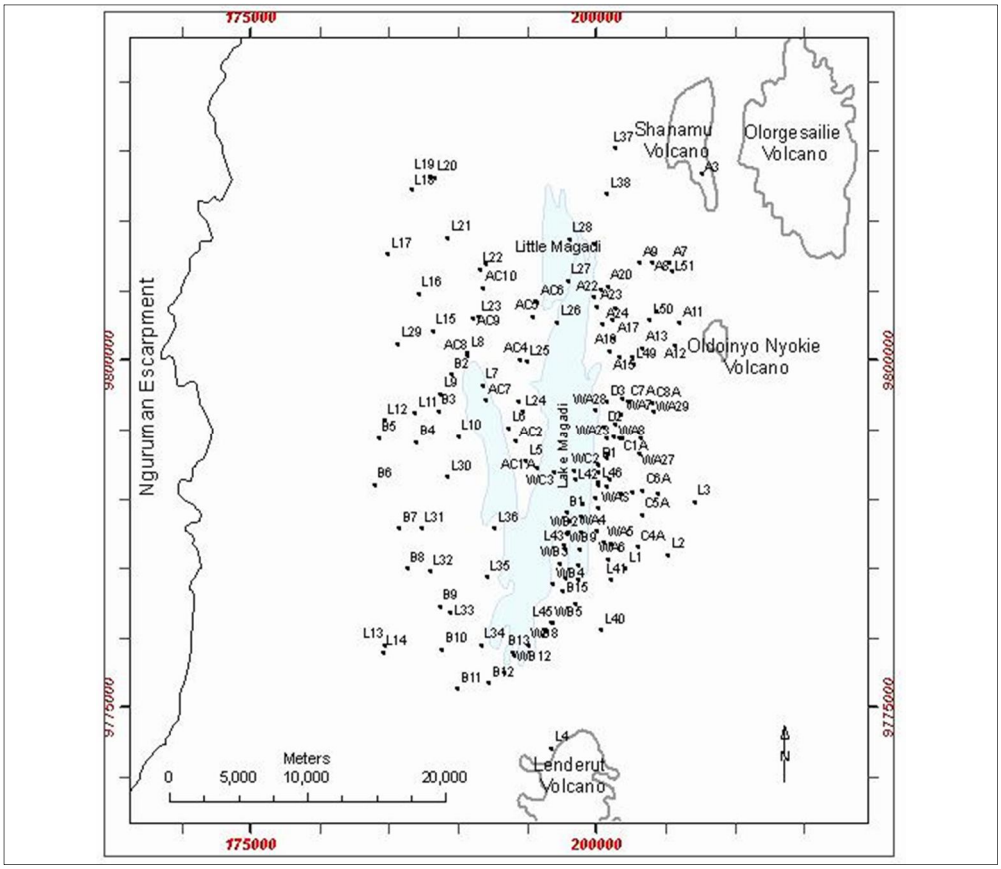

Figure 3: Gravity station distribution

The 1980 Geodetic Reference System (GRS80) (Moritz, 1980) was used in computing the normal gravity. The Somigliana formula (Somigliana, 1930) expressed as equation 1 was used to calculate for the theoretical gravity g_T.

$$g_\tau = \frac{g_e\left(1+kSin^2\varphi\right)}{\left(1-\varepsilon^2 Sin^2\varphi\right)^{\frac{1}{2}}} \quad \text{.....(1)}$$

where the GRS80 reference ellipsoid has the normal gravity at the equator (g_e) equal to 9.7803267715 m/s^2, k =0.001931851353 and ϵ^2 =0.0066943800229, where ϵ is the first numerical eccentricity. The theoretical gravity was calculated using this equation for each station latitude ϕ.

The free air anomalies, Δg_h, were computed from the second order approximation formula (Heiskanen and Moritz, 1969) in order to correct the theoretical gravity for a height (h) relative to the ellipsoid expressed as in equation 2.

$$\Delta g_h = -2\frac{g_e}{a}\left[1+f+m+\left(-3f+\frac{5}{2}m\right)\sin^2\varphi\right]h+\frac{3g_e h^2}{a^2}, \quad \text{.....(2)}$$

The following parameter values for the GRS80 ellipsoid were used: (a), the semi major axis, is 6378137 m; (b), the semi minor axis, is 6356752.3141 m; f, flattening, is 0.003352810681; g_e is 9.7803267715 m/s^2; and m, which is $\omega^2a^2b^2/GM$, is 0.00344978600308, where ω is the angular velocity (7292115x10^{-11} radians/sec) and the Product (GM) is 3986005 x 10^8 m^{3}s^2. The second order formula for the GRS80 ellipsoid is expressed as equation 3.

$$\Delta g_h = -\left(0.3087691 - 0.0004398\ Sin^2\theta\right)h + 7.2125 \times 10^{-8} h^2 \quad \text{.....(3)}$$

where the ellipsoidal height h is in metres and the gravity effect is in milligals. The Bouguer correction was calculated by assuming the earth between the vertical datum and the station to be represented by a horizontal slab using equation 4 (Mohr and Taylor, 2001).

$$\Delta g_{bc} = 2\pi G\sigma h = 4.193\,x10^{-5}\sigma h \quad \text{.....(4)}$$

where G, the gravitational constant, is 6.673± 0.001 x 10^{-11} m^3/kg/s^2, σ is the density of the horizontal slab in kg/m^3, and h is the height of the station in metres relative to the ellipsoid. Free-air and Bouguer gravity corrections were performed using sea level as the datum and a reduction density of 2.67 gcm^{-3}. The choice of this value results from attempts of Nettleton profiles (Nettleton, 1939) using density values ranging from 2.4 to 2.8 gcm^{-3}. A density of 2.67 gcm^{-3} had a Bouguer anomaly with least correlation to topography and was considered as the average crustal density. Terrain corrections were calculated using a Hammer chart constructed for zones D-J to a maximum radius of 5 km for all stations (Hammer, 1939). This was done using the topographic map sheets numbers 160/1, 160/2, 160/3 and 160/4 published by Survey of Kenya to a scale 1:50,000. The absolute gravity values at survey stations were obtained by reference to the International Gravity Standardization Network (IGSN), the Nairobi pendulum station (IGSN 71) (Morelli., 1974), station '35716 A', with an absolute gravity value of 9775260.7 g.u. However, IGSN71 values include a correction of the Honkasalo term (Honkasalo, 1964) which removes the average part of the tidal force. This correction term has been deemed inappropriate (Heikkinen, 1979) because of resulting errors in calculation of the geoid from gravity values corrected with the Honkasalo term. Therefore, following the recommendations of the International Association of Geodesy (Uotila, 1980), the Honkasalo term, Δg_h, was removed from all the observed gravity values that had been referenced to the IGSN71 station. This was done by adding a latitudinal varying correction in milligals given by equation 5.

$$\Delta g_h = 0.0371\left(1 - 3\sin^2\varphi\right), \quad \text{.....(5)}$$

where φ is the latitude south or north of the gravity station. This correction was effected by adding Δg_h to all the observed gravity values.

3.0 Bouguer Anomaly

Bouguer gravity anomaly maps are commonly used to investigate subsurface geology and structures (Blackely and Simpson, 1986). A complete Bouguer anomaly contour map at contour intervals of 5 mgals was plotted as illustrated in Figure 4.

The Bouguer anomaly map is characterised by long wavelength gravity low superimposed by positive anomalies. Several closed circular anomalies cluster the south-eastern part of the study area. Most of these anomalies are aligned in the NNE-SSW direction. The anomalies have high gradient which may be caused by shallow intrusives. Profiles AA', BB', CC', DD', EE' and FF' were plotted along the qualitatively discerned anomalies on the Bouguer anomaly map. A few low gradient anomalies are present in the same region also implying presence of deeper sources. The maximum anomaly amplitudes along the selected profiles AA', BB', CC', DD', EE' and FF' are -40 mgals, -50 mgals, 50 mgals, 40 mgals, 30 mgals and 10 mgals, respectively.

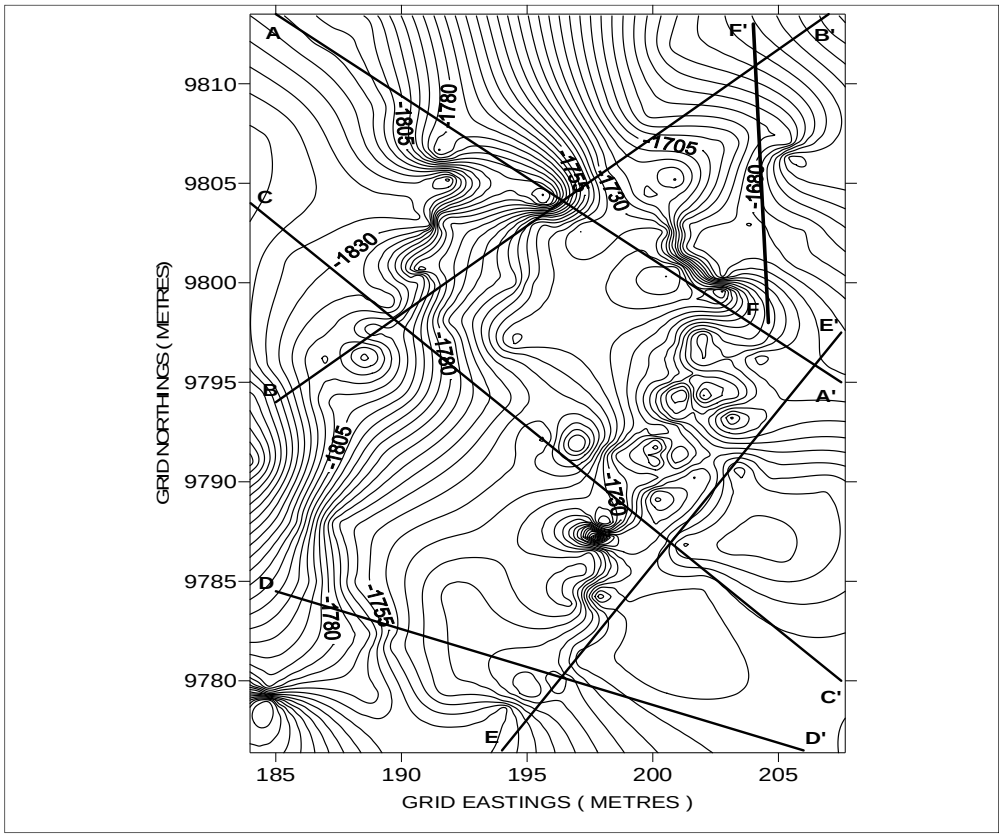

Figure 4: Bouguer anomaly contour map

4. 0 Euler Deconvolution Technique

Euler deconvolution is a technique, which uses potential field derivatives to image subsurface depth of a magnetic or gravity source (Hsu, 2002).

Mushayandebvu *et al.* (2001) described 2D space Euler's deconvolution using equation 6.

$$(X - X_0)\frac{\partial T}{\partial X} + (Z - Z_0)\frac{\partial T}{\partial Z} = -N\Delta T \quad \text{.....(6)}$$

where (X_0, Z) is the position of the top of the source, Z is the depth measured as positive down, X is the horizontal distance, ΔT is the value of the residual field, and N is the structural index. The structural index is a measure of the rate of change or fall off rate with distance of a field and therefore it is a function of the geometry of the causative bodies.

If ΔT_i is the residual field at the i^{th} point in a magnetic or gravity survey, with the point of measurement at (X, Z) and the centre of the body at (X_0, Z_0), then equation 6 can be expressed as matrix equation 7.

$$\begin{bmatrix} \frac{\partial}{\partial x}\Delta T_i & \frac{\partial}{\partial z}\Delta T_i \end{bmatrix}\begin{bmatrix} X - X_0 \\ Z - Z_0 \end{bmatrix} = N\Delta T_i \quad \text{.....(7)}$$

By calculating the horizontal and vertical gradients of the field, the equation 7 has only three unknowns X_0, Z_0 and N, where the first two describe the location of the body. Many simultaneous equations can be obtained for various measurement locations which may be simplified to one matrix illustrated as equation 8.

$$\begin{bmatrix} \frac{\partial}{\partial x}\Delta T_1 & \frac{\partial}{\partial z}\Delta T_1 \\ \frac{\partial}{\partial x}\Delta T_2 & \frac{\partial}{\partial z}\Delta T_2 \\ - & - \end{bmatrix}\begin{bmatrix} X - X_0 \\ Z - Z_0 \end{bmatrix} = N\begin{bmatrix} \Delta T_1 \\ \Delta T_2 \\ - \end{bmatrix}, \quad \text{.....(8)}$$

The least squares method can be used to obtain the unknowns X_0 and Z_0 if the structural index N is known. Software EULER 1.0, (Cooper, personal communication.) for carrying out two-dimensional Euler deconvolution was used to image gravity sources, where the 2D space defines depth (Z) positive down and horizontal distance (X). The source distribution is assumed to be two-dimensional such that the first derivatives of T that is $\frac{\partial T}{\partial X}$ and $\frac{\partial T}{\partial Z}$ at all the above locations are calculated by the software. When gravity data in a profile is run in EULER software, the profile is divided into windows of data points sets ranging from 7 to

19. A source location (X_0, Z_0) is calculated for each set of points using equation and least-squares methods. Source locations plotted in a cross-section clustered around magnetised sources.

Real data set is likely to contain anomalies from various geological features with varied structural indices. Therefore depth solutions for different structural indices (0.5, 1.0, 1.5, 2.0. 2.5 and 3.0) were obtained for each profile. The solution maps were examined and the index that gave the best cluster was chosen for the feature. This procedure also gave an idea about the nature of the causative feature. The solutions generated for single data sets showed that imaged depth increased with increasing assumed structural index.

5.0 Boundary Analysis by Horizontal Gradients

The horizontal gradient is given by equation 9.

$$h(x,y)=\left[\left(\frac{\partial g_z(x,y)}{\partial x}\right)^2+\left(\frac{\partial g_z(x,y)}{\partial y}\right)^2\right]^{\frac{1}{2}} \quad \text{.....(9)}$$

The steepest gradient is located over the edge of the body if the edge is vertical and far removed from all other edges or sources. This characteristic of gravity anomalies is useful in locating abrupt lateral changes in density from gravity measurements (Cordel, 1979). The assumption in this procedure is that the contrasts in density occur across vertical and abrupt boundaries isolated from other sources.

6.0 Discussion of Euler Deconvolution and Gradients Results

From gravity profile AA' in Figure 5, the gravity anomalies in the profile is superimposed and may represent multiple features. A structural index of 0.5 was used which best represents dike structures. Maximum depth imaged along the profile is approximately 2 km while the shallowest is almost to the surface. Most solution cluster is at a profile distance ranging 14 km to 21 km. From 17 km to 26 km, the gravity anomaly displays a gravity low with a high superimposed at about 21.5 km. This may represent high-density material impregnated in relatively low-density material.

From gravity profile BB' in Figure 6, it is a gravity low superimposed by a high at a profile distance of 5 km. The most conspicuous lows are at profile distances 7 km and 15 km with corresponding imaged depths of approximately 0.5 km and 0.7 km respectively. The lows also coincide with solution cluster. Major discontinuities are observed from 8-20 km and from 24-26 km. Abrupt change in both horizontal and vertical gradients was observed from 4-5 km, 5-7 km, 14-15 km, 17-18 km and 24-25 km which most probably represents lateral change in magnetisation. Depths to the gravity structure displayed are rather shallow ranging from 0.2-1.5 km.

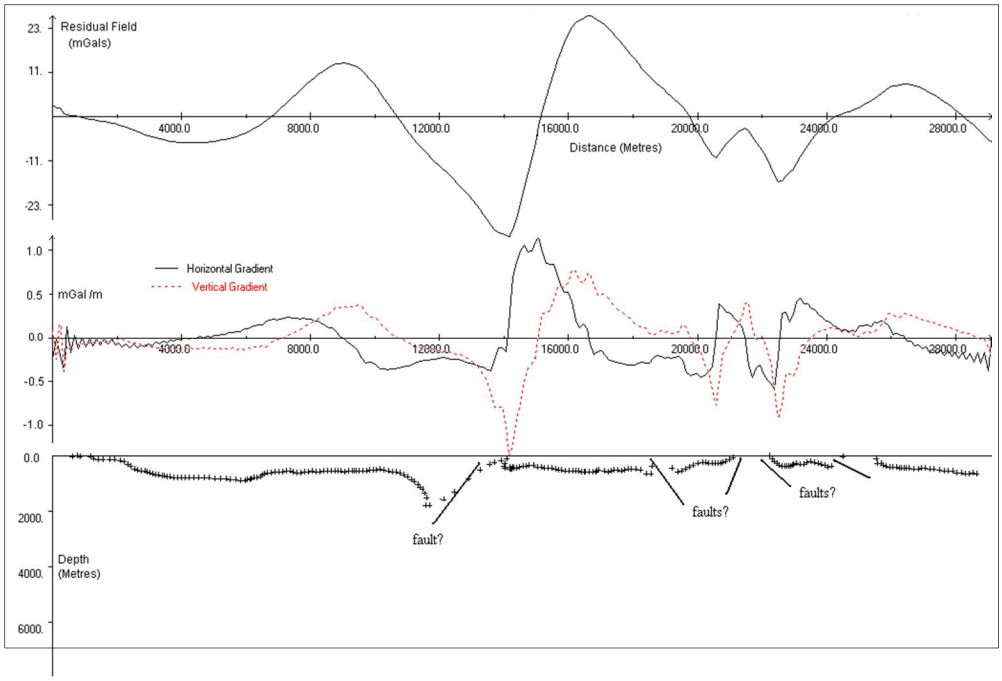

Figure 5: Euler depth solution for profile A-A'.

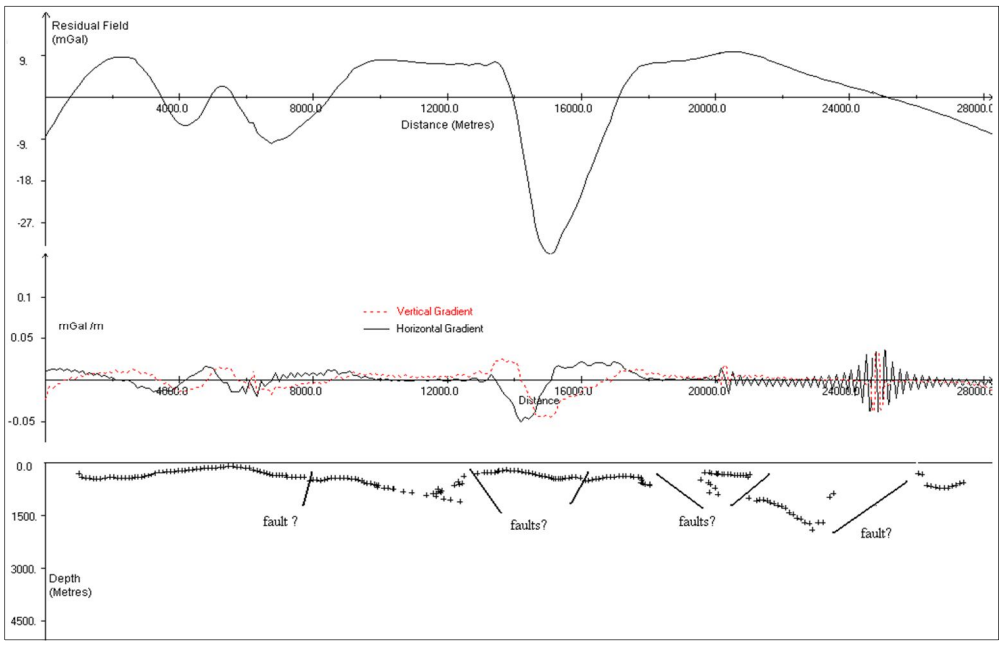

Figure 6: Euler depth solution for profile BB´

The gravity profile CC' in Figure 7 is a gravity high superimposed by local lows at 7.5 km, 18 km and 25 km. The imaged depth solutions also indicated several

discontinuities at horizontal profile distances 5-7 km, 14-15 km, 18-20 km and 22.5 km. Maximum depth imaged is approximately 1.5 km with the shallowest being close to the surface.

The gravity profile DD' in Figure 8 is a long wavelength gravity high superimposed by local gravity lows at horizontal profile distances of 4 km and 12 km respectively. The Euler solutions indicate a discontinuity at a horizontal profile distance of 6-9 km, which may be indicative of faulted structure. Gravity profile EE' in Figure 9 displays a long wavelength gravity high with fluctuating lows. Sharp changes in gradients are observed at 4 km, 8 km, 12 km and 16 km. The deepest depth imaged is 1.5 km and the shallowest close to the surface.

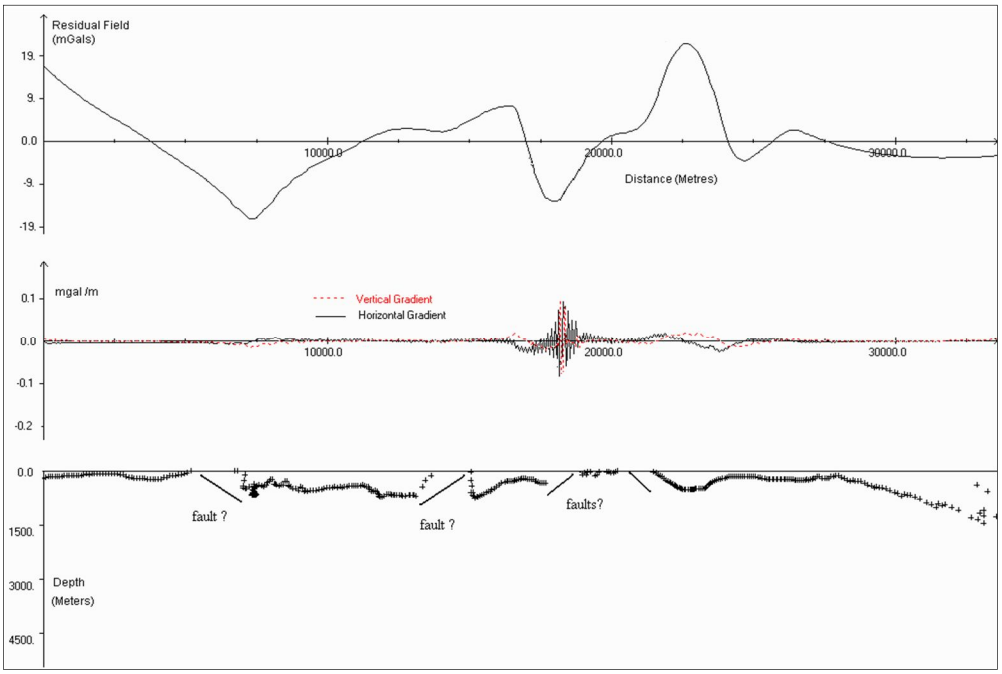

Figure 7: Euler depth solution for profile C-C'

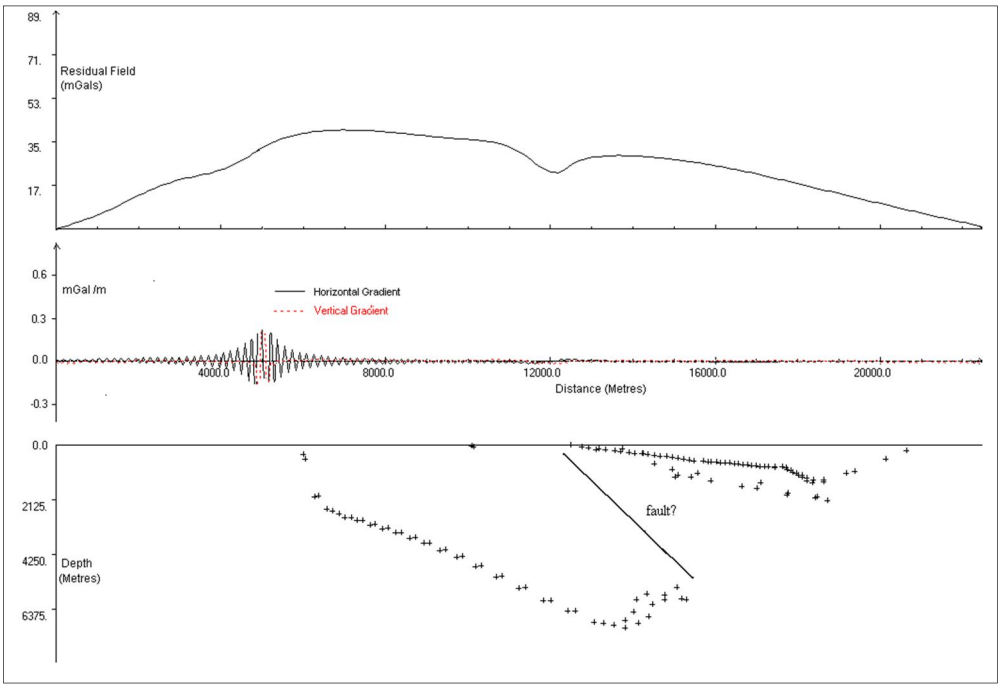

Figure 8: Euler depth solution for profile DD´

The gravity profile FF' in Figure 10 has a positive anomaly with an amplitude of about 10 mgals and a negative anomaly at 4 km and 10 km horizontal profile distances respectively. Discontinuities are also observed at a profile distance of 3-4 km.

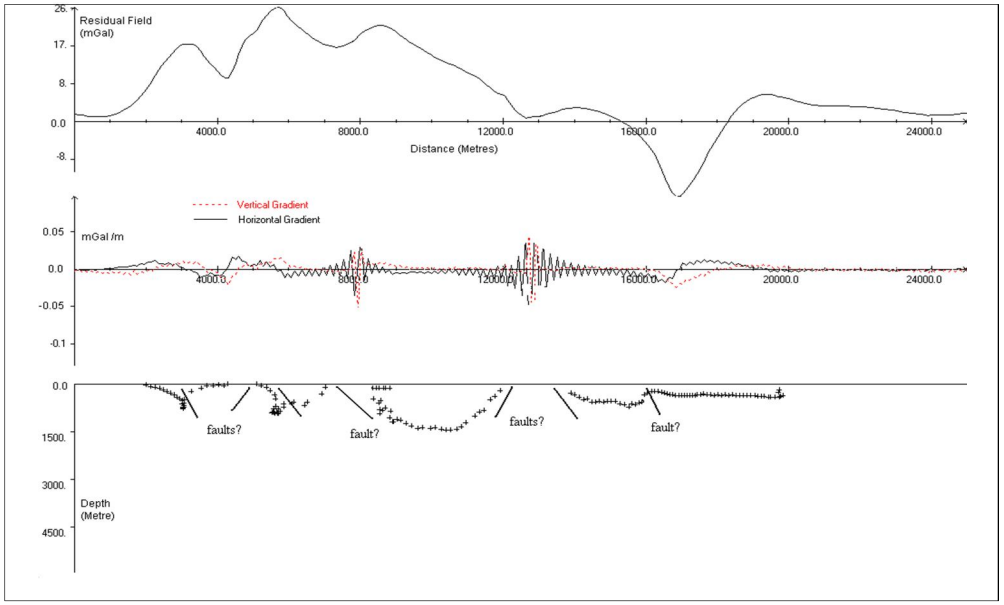

Figure 9: Euler depth solution for profile EE´

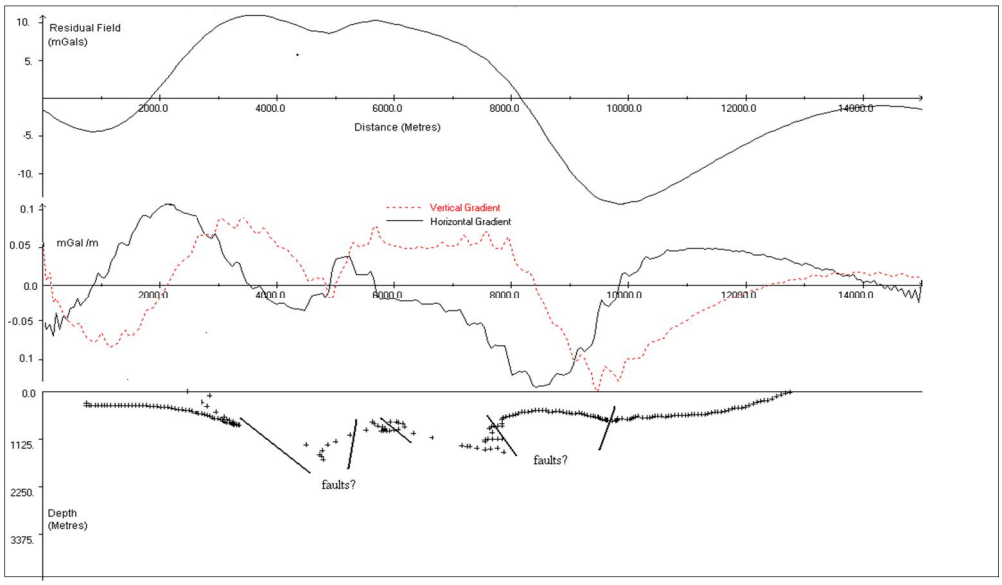

Figure 10: Euler depth solution for profile FF´

7.0 Forward Modeling of Gravity Data

To better understand the geometries and densities contrasts of the causative bodies, forward 2-D modeling for gravity data was done along the selected profiles using the software Grav.2dc (Cooper, personal communication). This software was used to calculate gravitational attraction at each observation point due to polygonal shaped bodies, with each body having a specific density. In this method, the 2-D arbitrary body is assumed to have an infinite strike length. A body is approximated by polygons whose gravity effects are summed up by numerical integration using the algorithm inGrav.2dc software. The interactive nature of these software allowed adjustment of the initial start model until an acceptable fit was obtained for the models. The initial body geometries for the modeling process were based on results from Euler deconvolution. The start parameters derived from Euler results were depth and shape of causative body inferred from the structural index used. As a control, the same density contrast was assigned to bodies above which any two profiles crossed over.

From gravity survey along line G of the KRISP 94 experiment that traversed through Magadi, Birt *et al.* (1997) assigned the near surface sediments and volcanics densities ranging from 2.4 to 2.6 g cm^{-3}. Simiyu (1996) modeled shallow basin structures in the southern Kenyan rift valley by assigning the average density of 2.3 to 2.4 gcm^{-3} for the rift graben fill. Assuming an average crustal density of 2.67 g cm^{-3} in the rift valley as had been deduced from Nettleton's near surface method (Nettleton, 1939), a density contrast of -0.27 g cm^{-3} was used for near surface sediments. Birt *et al.* (1997) also assigned basement densities ranges of 2.68 to 2.80 gcm^3 and mid crustal units a range of 2.84 to 2.86 g cm^3. Hay *et al*.

(1995) had also modeled the Kenya Rift Ponolites and the lowest crustal unit had a density of 2.95 g cm^{-3} outside the rift and 3.0 g cm^{-3} beneath the active rift zone. This was also used as a control to the density contrasts to avoid unrealistic contrasts.

8.0 Discussion of Forward Modeling Results

The gravity model along profile AA' in figure 11 displays three peaks of highs corresponding to relatively denser bodies of density contrasts 0.257, 0.5335 and 0.288 g cm^{-3}. The first and third are within the range as for crustal material as assigned by Birt *et al*. (1997). The gravity high located at a profile distance of 16.7 km has the highest density contrast of 0.5335 g cm^{-3}. Assuming the contrast is relative to average crustal density of 2.67 g cm^{-3}, then the absolute density of the body responsible is 3.20 gcm^{-3} which may be mantle material and most likely an intrusive. From the profile AA' of the gravity model the near surface sediments range from a depth of approximately 0.2 km to 2 km for the gravity model. The sediments were modeled to have density contrast of -0.270 gcm^{-3}.

The gravity model along profile BB' illustrated by figure 12 has three prominent gravity highs of density contrasts 0.2349. 0.4185 and 0.5335, which corresponds to densities of approximately 2.90, 3.01 and 3.20 respectively. The first density represents lower crust materials while the second or third may represent mantle material. The low situated at 7 km profile distance corresponds to a basin to a depth of up to 1km filled with sediments. The gravity low at 18.5 km may represent unconsolidated sediments. Gravity high located 23.5 km is also modeled to have a density of 3.20 gcm^{-3}.

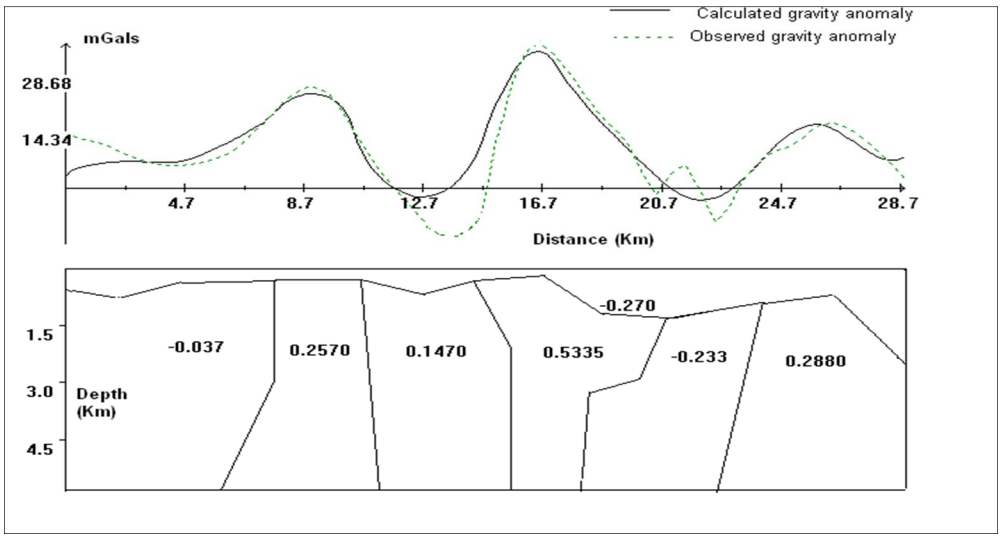

Figure 11: Gravity model along profile A-A'

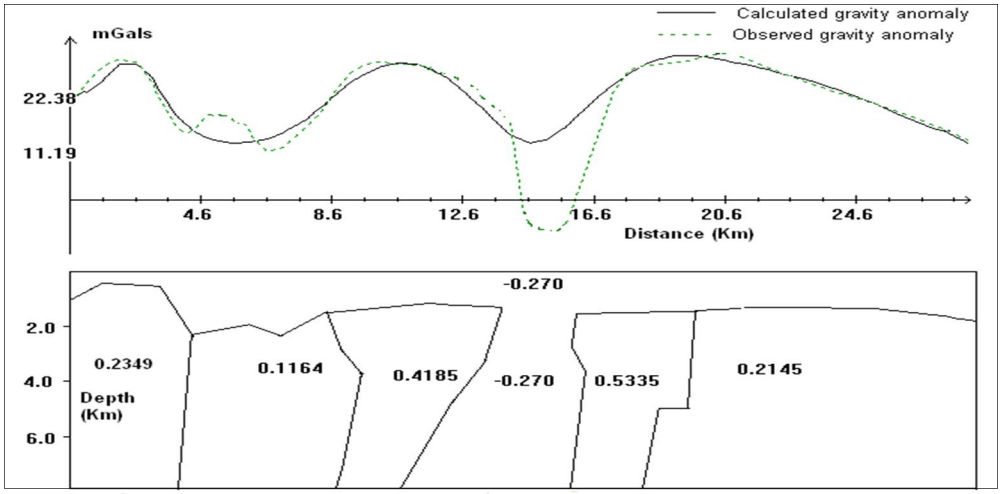

Figure 12: Gravity model along profile B-B'

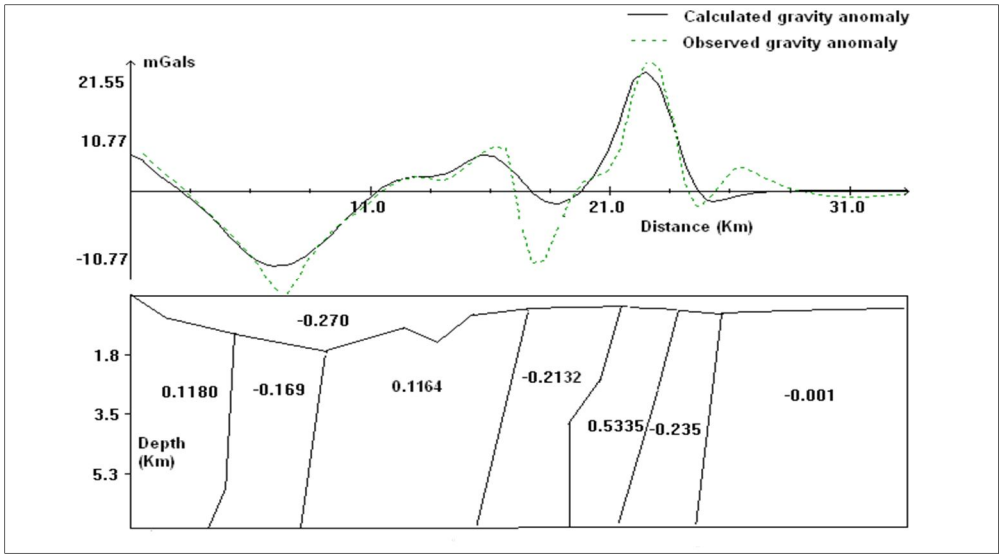

Figure 13: Gravity model along profile C-C'

Gravity profile DD' in figure 14 consists of a long wavelength gravity high superimposed by a gravity low. This high was modeled to consist of a rock of density 3.07 gcm^{-3} impregnated by a material of density 2.445 gcm^{-3}. These may be unconsolidated sediments. Gravity profile EE' in figure 15 has a high of density 2.88 gcm^{-3} at 6.8 km and a low of 2.4 gcm^{-3} extending from the surface to a depth of more than 5 km. These are lake sediments occurring at Lake Magadi.

At a distance of 11.4 km along profile EE' as illustrated by figure 15, a body is modeled with low density contrast. This feature had previously been mapped by Githiri *et al,* (2004) and interpreted as magnetized sediments. Along profile FF'

from figure 16, the sediments from the surface extends up to a maximum depth of 3 km. A gravity high centered at 5.4 km is due to a body of density 2.95 gcm^{-3} which is possibly an intrusive. At 10.4 km profile distance, the gravity model has a low which may be contributed to by a deeper sediment basin underlain by volcanics of density 2.545 gcm^{-3}

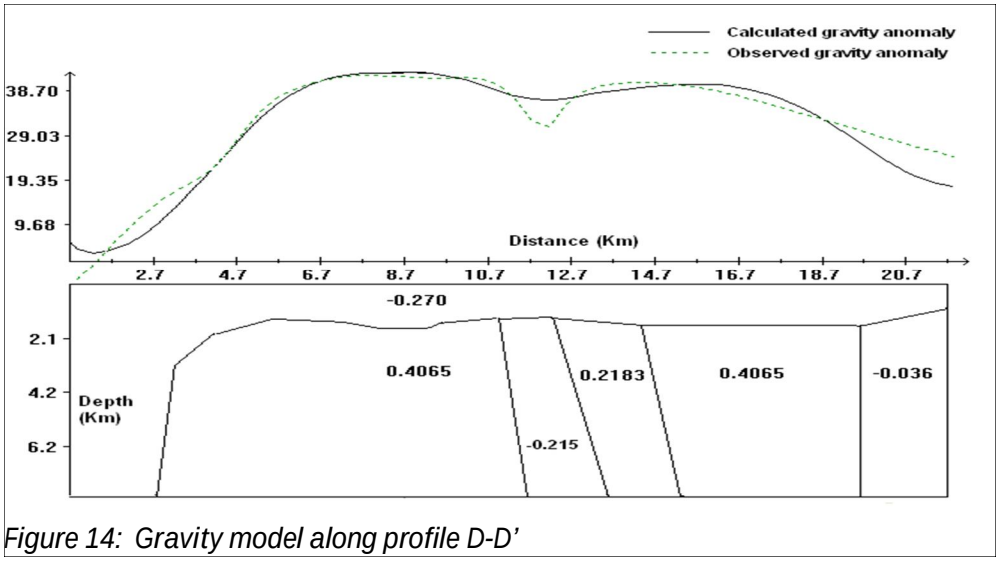

Figure 14: Gravity model along profile D-D'

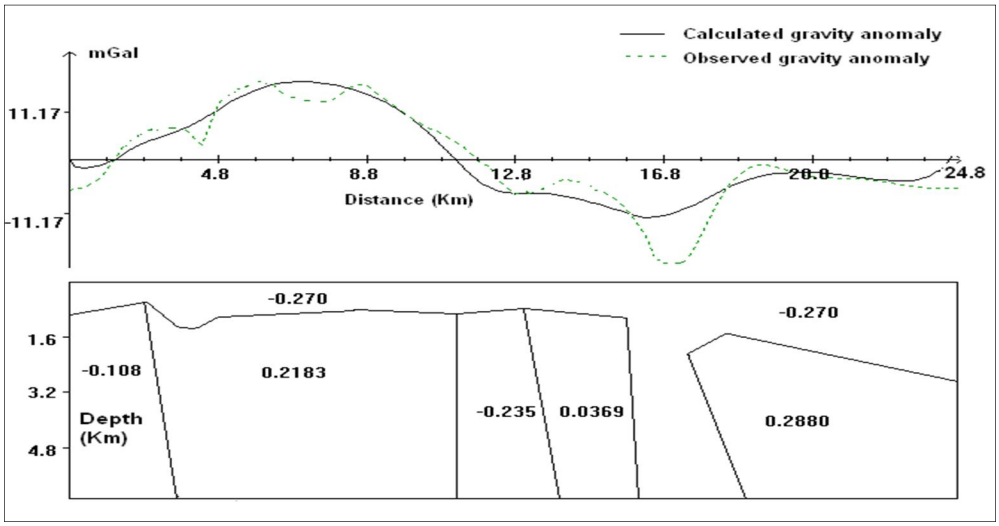

Figure 15: Gravity model along profile E-E'

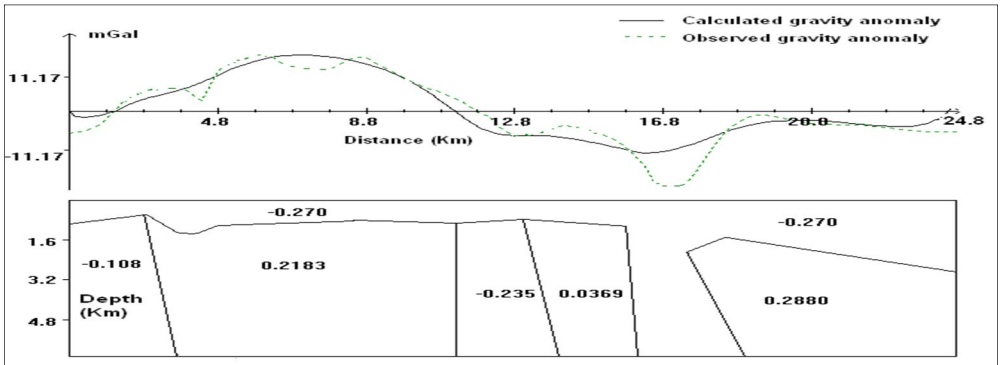

Figure 16: Gravity model along profile F-F'

9.0 Conclusion

The application of gravity prospecting methods in Magadi has revealed presence of bodies with density contrast that may be magmatic intrusions. The most prominent such bodies transacted by both profiles AA' and BB' is centred at location with UTM coordinates (196, 9805) and another by profile CC' centred at coordinates (197, 9789) as illustrated in figure 4. They are both modelled to have density of 3.20 gcm^{-3} as in figures 11, 12 and 13. From the seismotectonic study by Ibs-Von Seht *et al* (2001), a locally up-warped brittle-ductile transition was found to occur at a depth of 15 km in the south and 10 km in the north. This confirms presence of a low shear strength material at a relatively shallower depth northward than southward. The location of the earthquake swarms is traversed by profile AA' on the northern region and coincides in position to the body modelled with the high density contrasts. Discontinuities in Euler solution cluster along the profiles indicated buried faults in the volcanic rift infill. Therefore from the results of this study, the detected relatively shallow intusives of high density at high temperature may be emanating from a magma chamber. The hot magma penetrates through the rocks increasing stress which on release causes the earthquakes observed in studies by Ibs-Von Seht et al (2001). Chances of an occurrence of a major earthquake are still high as the hot magma is continually increasing strain in the rocks.

Acknowledgements

Special thanks to the staff of the Physics department of Jomo-Kenyatta University of Agriculture and Technology (JKUAT) for their valuable suggestions in this study. Also we are grateful to Geomatic Engineering department of JKUAT for allowing us to use their Maps and digitizing equipment. We are also grateful to Professor Cooper of University of Witwatersrand for providing Euler 1.0 and Grav 2dc software used in this work. This study was jointly funded by JKUAT under the division of Research, Production and Extension and National Council for Science and Technology (NCST).

`

References

Atmaoui N. (1999). Structural analysis of neotectonic joints at Lake Magadi area and their relationship with regional faults using remote sensing imagery interpretation. M.Sc thesis, University of Nairobi, pp 100-101.

Baker B. H. (1958). Geology of the Magadi area. Report Geological survey of Kenya 42. The Government printer, Nairobi.

Baker B. H. (1963). Geology of the area south of Magadi. Report Geological survey of Kenya 61. The Government printer, Nairobi.

Baker B. H. (1986). Tectonics and Volcanism of the Southern Kenya Rift valley and its influence on rift sedimentation. In: Frostick L. E. et al. (eds) 1986, sedimentation in the African Rifts. Geol. Soc. Spec. Publ. No 25, pp 45-47.

Birt C. S, Maguire P. K. H., Khan M. A., Thybo H., Keller G. R., Patel J. (1997). *The influence of pre-existing structures on the evolution of the southern Kenya rift valley- evidence from seismic and gravity studies.* Tectonophysics, **278**, pp 211-242.

Blakely R. and Simpson R. (1986). *Approximating edges of source bodies from magnetic or gravity anomalies.* Geophysics, **51**, pp 1494-1498.

Cordell L., (1979). Gravimetric expression of graben faulting in the Santa Fe country and the Espanola Basin, New Mexico. Guide book to Santa Fe country, 30th field conference, R. V Ingersol (ed), New Mexico Geological society, pp. 59-64.

Crossley R., (1979). Structure and volcanism in the southern Kenya Rift. In Geodynamic evolution of the Afro- Arabian Rift System. Acad. Nazionale dei Lincei, Rome, pp 89-98.

Githiri J. G., Stangl R. L., Waithaka J. W. and Dindi E. W., (2004). *Ground magnetic survey of Magadi geothermal field.* East African journal of Physical sciences, **5**(2), pp 69-80.

Hammer S., (1939). *Terrain corrections for gravimeter stations*. Geophysics.,*4,* pp 184-194.

Hay D. E., Wendlandt R. F. and Keller, G. R., (1995). *Origin of Kenya Rift plateau-type phonolites: Integrated petrological and geophysical constraints on the evolution of the crust and upper mantle beneath the Kenya Rift*.J. Geophys. Res. **100**, pp 10549-10557.

Heikkinen M. (1979). *On the Honkasalo term in tidal corrections to gravimetric observations:* Journal of Geodesy, **53**, pp 239-245.

Heiskanen W. A., and Moritz H., (1969). Physical geodesy: W.H. Freeman Co.
Honkasalo T., (1964), On the tidal gravity correction: Bulletin of Theoretical and Applied Geophysics, **6**, pp 34-36.

Hsu Shu-Kun (2002). *Imaging magnetic sources using Euler's equation*. Geophysical prospecting Vol. 50, pp 15-25.

Ibs-Von Seht M., Blumenstein S., Wagner R., Hollnack D. and Wohlenberg J. (2001). *Seismicity, Seismotectonics and Crustal structure of the southern Kenya Rift-new data from Lake Magadi area.* Geophys.J Int. Vol. 146, pp 439-453.

Khan M. A., and Swain, C. J. (1977). A catalogue of Gravity measurements in Kenya. Department of Geology, Leicester Univ., pp 21-22.

Mohr P. J., and Taylor B. N. (2001). The fundamental physical constant: Physics Today, **54**, pp 6-16.

Morelli C., (1974). The International Gravity Standardization Net 1971: International Association of Geodesy, Special Publication 4.

Moritz H. (1980). *Geodetic Reference System 1980*: Journal of Geodesy, **54**, pp 395-405.

Mushayandebvu M. F., Van Driel P., Reid A. B. and Fairhead J. D., (2001). *Magnetic source parameters of two-dimensional structures using extended Euler deconvolution:* Geophysics, **66**, pp 814-823.

Nettleton L. L. (1939). *Determination of density for reduction of gravimeter observations*. Geophysics, Vol. 4 pp 176-183.

Simiyu S. M. (1996). Intergrated geophysical study of the crustal structure of the southern Kenya Rift, East Africa. Tectonics, **12**, pp 591-606.

Smith M. (1994). *Stratigraphic and structural constraints on mechanisms of active rifting in the Gregory Rift, Kenya,* in; Prodehl C., Keller G. R and Khan M. A (editors), crustal and upper-mantle structure of the Kenya Rift, Tectonophysics, **236**, pp 3-22.

Somigliana C. (1930). *Geofisica-SuI campo gravitazionale esterno deI geoide ellissoidico: Atti della Accademia nazionale dei Lincei. Rendiconti.* Classe di scienze fisinche, matematiche e naturali, **6**, pp 237-243.

Uotila U. A. (1980). *Note to users on International Gravity Standardization Net 1971:* Journal of Geodesy, **54**, pp 407-408.